Lasers in Manufacturing Conference 2021

Femtosecond laser structuring of nodular cast iron for anti-corrosion and thermally stable superhydrophobic surface

Dhiraj Kumar[a,*], Karla Kroechert Ching[b], Georg Kalss[b], Gerhard Liedl[a]

[a] *Institute of Production Engineering and Photonic Technologies, TU Wien, Franz Grill Strasse 9, Vienna 1030, Austria*
[b]*Department of Research and Development, Bühler Group, Leobendorf 2100, Austria*

Abstract

The superhydrophobic surface has many applications, such as anti-corrosion, anti-icing, and self-cleaning. In this paper, we describe superhydrophobic surfaces on nodular cast iron produced by femtosecond laser pulses. A rapid transformation of surface characteristics from hydrophilic to superhydrophobic has been achieved after placing the samples in a high vacuum chamber for 10 hours, indicating a significant reduction in the storage time required to develop hydrophobic properties. Thermal stability has been assessed after heating the samples at different temperatures for an hour in a furnace. Consequently, the static contact angle has been measured after cooling at room temperature. Samples irradiated at 0.63 J/cm^2 and 3.18 J/cm^2 with a hatch distance of 20 µm show stable superhydrophobic characteristics up to 180°C. Corrosion tests have also been carried out on untreated and laser-treated samples at room condition in a 3.5% NaCl solution. Results indicate that a superhydrophobic surface has better resistance toward corrosion.

Keywords: Femtosecond laser; Superhydrophobic; LIPSS; Thermal stability; Corrosion

1. Introduction

The femtosecond laser ablation process has received much attention due to its precise removal of materials with no molten or recast layer and the capability to fabricate micro to nanoscale topographies on a range of materials metals, polymers, glass, semiconductors, composites, and ceramics, as mentioned by **Birnbaum, 1965**. The ablation threshold of materials and their ablation rate is considered an effective parameter in the femtosecond laser micro/nano-structuring to produce uniform laser-induced periodic surface structures (LIPSS) by **Ahmed et al., 2014**. LIPSS morphology and its properties, such as optical, wetting, and tribological, have been severely influenced by the laser parameters such as fluence, the number of pulses,

* Corresponding author.
E-mail address: Dhiraj.kumar@tuwien.ac.at.

scan speed, wavelength, repetition rate, and pulse duration, as mentioned by **Zemaitis et al., 2020**. Ultrafast laser-induced superhydrophobic surfaces have many applications in recent times, particularly; when anti-icing, self-cleaning, thermally stable, and anti-corrosion are considered the prime requirement.

Nodular cast iron (NCI) has received significant attention from the industries such as automotive, wind, and automobile industries due to the specific advantages, e.g., high ductility, strength, resistance to shock, corrosion, and wear. Due to better castability, machinability, and high recycle efficiency, NCI has been used for low to mid-range stressed components for various applications, as stated by **Hamberg et al., 1997**. Improving hydrophobicity of the NCI surface is the primary concern that could be enhanced by producing a hierarchical micro/nano-structure using a femtosecond laser. The present investigation focuses on the applicability of the femtosecond laser to create a superhydrophobic surface on the NCI substrates. Static contact angle (SCA) has been measured to characterize the behavior of the surface over time and after the vacuum process. Thermal stability of superhydrophobic surface has been assessed after heating for an hour in a furnace. Resistance toward corrosion characteristics of produced surfaces has also been carried out, performing an electrochemical test in a 3.5% NaCl.

2. Materials and methods

2.1. Materials

Femtosecond laser structuring is performed on NCI samples provided from Bühler Group, Leobendorf, Austria. The detailed chemical composition of the NCI sample is presented in table 1. Laser structuring is done in a 5 mm × 5 mm area on a sample size of 40 mm × 40 mm × 9 mm. Before the structuring, samples are placed in ethanol (99.9%) and sonicated for 30 min at room temperature to remove the attached residues.

Table 1. Elemental composition of NCI samples (in percentage).

Sample	C	Mn	Si	P	S	Cu	Mg	Fe
NCI	3.61	0.33	2.25	0.02	0.005	0.269	0.041	Balance

2.2. Femtosecond laser and process parameters

Ti-sapphire laser with an average power of 800 mW, operated at 1000 Hz repetition rate with 30 fs pulse duration, and 800 nm center wavelength (λ) was used to produce hierarchical micro/nano-structuring on NCI samples. Line scanning was performed, keeping hatch distances of 20 and 40 µm at a fluence of 0.63 J/cm^2 and 3.18 J/cm^2 with a scan speed of 1.0 mm/s. The smallest, in focus, beam spot size is 35 ± 5 µm; experiments were performed in focus. Further, treated NCI samples were sonicated for 30 min in ethanol to clean the attached residues.

2.3. Surface characterizations

SCA was measured using an OCA 25 supplied by Dataphysics, Germany. SCA measurement was done at room temperature using the sessile drop technique with 3 µL of deionized water droplet doses at a dispense

rate of 1 µL/s. SCA was measured with an equal interval of air exposure time and after the vacuum processing to observe the influence of the secondary process (vacuum process) on the hydrophobicity of irradiated NCI.

The thermal stability of produced superhydrophobic surface was investigated after heating samples at 120°C to 180°C in a furnace for an hour. When samples were cooled down to room temperature, their corresponding SCA was measured and reported for analysis. Samples irradiated at 0.63 J/cm^2 and 3.18 J/cm^2 with a hatch distance of 20 µm were considered for thermal stability. A corrosion test of the untreated and superhydrophobic surface was conducted using an electrochemical process in a 3.5 % NaCl electrolyte solution. Before the electrochemical investigation, the working electrode was introduced into the test solution and was allowed to attain a steady-state potential. Then a potential range of -600 mV to – 50 mV with a scan rate of 1 mV/s was applied, and corresponding corrosion potential (E_{corr}) and corrosion current density (I_{corr}) were obtained from the potential (E) vs. log I curves by the Tafel extrapolation method. Scanning electron microscopy (SEM) was carried to observe the generated micro/nano-structure before and after performing corrosion tests.

3. Results and discussions

3.1. SCA variation with time and vacuum process

Figure 1 presents the variation of SCA with days and after application of the vacuum process. The sample indicates a gradual increase in SCA over the days. It achieves a maximum value of 158.6° and 81° after 60 days of air exposer when treated at a fluence of 3.18 J/cm^2 with a hatch distance of 20 and 40 µm, respectively. The sample structure with a hatch distance of 20 µm has achieved saturation that indicates the significant influence of hierarchical structure on the SCA. Afterward, when the sample has been placed in a vacuum chamber for 10 h, a substantial increase in SCA is observed, particularly with a hatch distance of 40 µm. **Dhiraj et al., 2020** mentioned that rapid absorption of hydrocarbons or non-polar functional groups from the vacuum chamber could be a reason. However, the vacuum process has a marginal impact on the saturated samples. A similar observation has been made by **Sciancalepore et al., 2018** that witnessed a steep increase in SCA initially and is saturated over the few more days of air exposer. This may be the one reason when samples are processed in a vacuum but have limited influence on SCA.

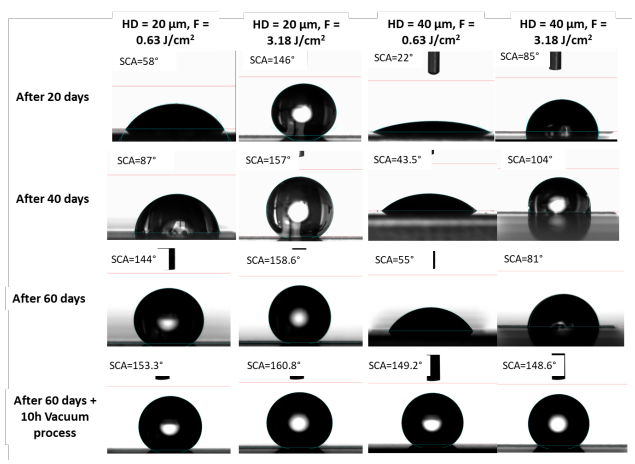

Fig. 1. Variation of SCA with days and after applications of vacuum process.

3.2. Thermal stability

Figure 2 presents the results after thermal stability analysis of samples irradiated at 0.63 J/cm^2 and 3.18 J/cm^2 with a line scanning width of 20 µm. Initially, samples are heated in a furnace at 120°C for an hour afterward placed in an open environment. As soon as samples cooled to room temperature, corresponding SCA is measured. A similar approach was used for other temperature levels. SCAs of irradiated samples were 153.3° and 160.8° for 0.63 J/cm^2 and 3.18 J/cm^2, respectively, before the thermal stability experiment (see figure 1). One can notice that SCA increased with an increasing temperature to 150°C and achieved its highest value to 163.8° and 164.8°, respectively, for the fluence of 0.63 J/cm^2 and 3.18 J/cm^2**. Ngo and Chun, 2018** stated that the low-temperature annealing process leads to increased hydrophobicity have made similar observations. The annealing process might be accelerating the absorption of an organic functional group from the atmosphere when placed in the air. Moreover, a marginal drop in SCA is noticed with a further increase in temperature; however, surfaces do not change their behavior and retain superhydrophobicity.

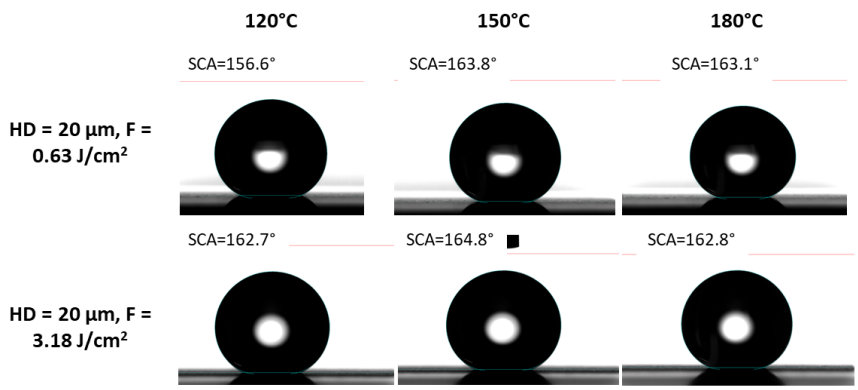

Fig. 2. Thermal stability of superhydrophobic surface

3.3. Electrochemical process

An electrochemical test in 3.5 wt% of NaCl is performed on the treated and untreated samples. Correspond I_{corr} and E_{corr} are presented in table 2, obtained from the polarization curve (see figure 3 (a)). Generally, a lower value of I_{corr} and a higher value of E_{corr} *are* considered better corrosion resistance. Figure 3 (a) shows that a superhydrophobic surface obtained after laser structuring at 3.18 J/cm^2 with a hatch distance of 20 µm and a scan speed of 1 mm/s provides better resistance towards corrosion due to poor wetting behavior. However, the superhydrophilic surface (hatch distance = 40 µm, fluence = 3.18 J/cm^2, scan speed = 0.2 mm/s, position = in focus) is more prone to corrosion and witnesses high current density compared to the superhydrophobic surface. SEM micrograph shows maximum damage to the superhydrophilic surface; moreover, less corroded or damaged surface observed on as produced superhydrophobic surface (see figure 3 (b)). Figure 4 indicates the SCA values before and after the corrosion test. SCA decreased significantly after the corrosion test, particularly for superhydrophobic surfaces; however, SCA observed no change with superhydrophilic surfaces. The untreated surface is also showed declined in SCA after performing the corrosion test.

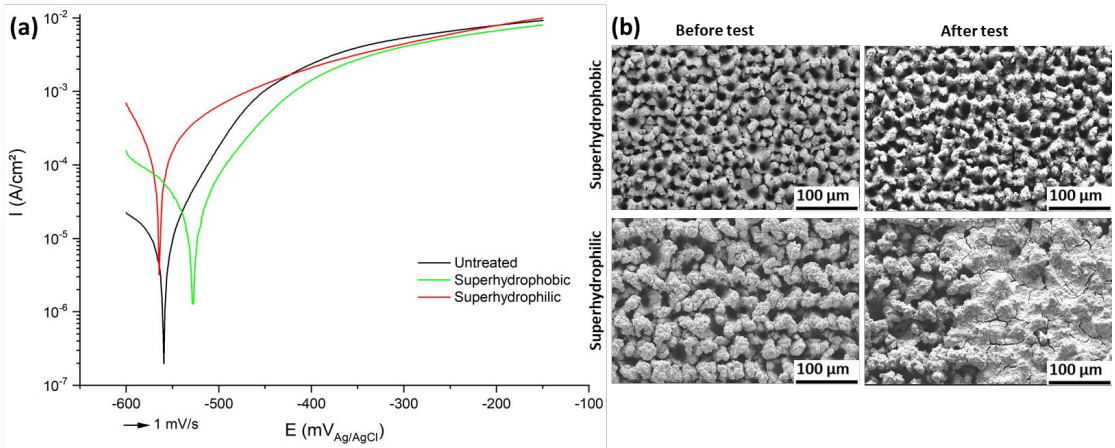

Fig. 3. (a) Polarization curve obtained after electrochemical test and (b) SEM micrograph of samples before and after the test.

Table 2. Values for corrosion parameters obtained from the curve.

Samples	I_{corr} (A/cm^2)	E_{corr} (mV/Ag/AgCl)
Untreated	5.30×10^{-5}	-558
Superhydrophobic	2.78×10^{-5}	-526
Superhydrophilic	2.02×10^{-4}	-563

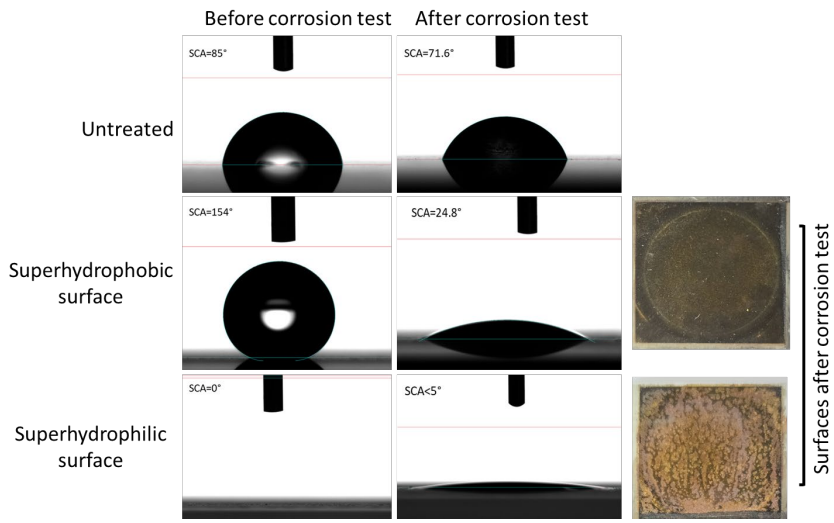

Fig. 4. SCA of samples before and after the corrosion test.

4. Conclusions

NCI samples were irradiated with femtosecond laser at a fluence of 0.63 J/cm^2 and 3.18 J/cm^2 with a scan speed of 1 mm/s and line scan width of 20 and 40 µm. SCA increases over the days; moreover, the vacuum process rapidly increases the SCA. Hierarchical structures achieve superhydrophobic behavior quickly; on the other hand, irregular or micro-structures have taken a long time to show hydrophobicity. A thermally stable superhydrophobic surface has been achieved that retains its characteristics even after heating at 180°C for an hour. The superhydrophobic surface has shown better resistance towards corrosion during the electrochemical test. However, SCA decreased significantly after the corrosion test.

Acknowledgment

The authors would like to thank the University Service Centre for Transmission Electron Microscopy (USTEM), Vienna University of Technology, Austria for SEM micrograph and Günther Ball from the Institute for Chemical Technologies and Analytics (TU Wien) for carrying out the electrochemical corrosion tests. This work was partially funded by Österreichische Forschungsförderungsgesellschaft FFG (Project No. 874745).

References

Ahmed, K. M. T., Grambow, C., Marie-Kietzig, A., 2014. Fabrication of Micro/Nano-Structures on Metals by Femtosecond Laser Micromachining. Micromachines 5(4), p. 1219-1253.

Birnbaum, M., 1965. Semiconductor surface damaged produced by ruby lasers. Journal of Applied Physics 36, p. 3688-3689.

Hamberg, K., Johannesson, B., Robertson, A., 1997. Defect sensitivity in nodular cast iron for safety critical components. European Structural Integrity Society 22, p. 37-47.

Kumar, D., , Liedl., G., Gururaja, S., 2020. Formation of sub-wavelength laser induced periodic surface structure and wettability transformation of CFRP laminates using ultra-fast laser. Materials Letters 276, p. 128282.

Ngo, C. V., Chun, D. M., 2018. Effect of heat treatment temperature on the wettability transition from hydrophilic to superhydrophobic on laser ablated metallic surfaces. Advanced Engineering Materials 20, p. 1-11.

Sciancalepore, C., Gemini, L., Romoli, L., Bondioli, F., 2018. Study of the wettability behavior of stainless steel surfaces after ultrafast laser texturing. Surface and Coatings Technology 352, p. 370-377.

Zemaitis, A., Mimidis, A., Papadopoulos, A., Gecys, P., Raciukaitis, G., Stratakis, E., Gedvilas, M., 2020. Controlling the wettability of stainless steel from highly-hydrophilic to super-hydrophobic by femtosecond laser-induced ripples and nanospikes. RSC Advances 10, p. 37956-37961.